Nanostructure and local polymorphism in "ideal-like" rare-earths-based high-entropy alloys

Andreja Jelen[a], Jae Hyuck Jang[b], Junhyup Oh[b], Hae Jin Kim[b], Anton Meden[c], Stane Vrtnik[a], Michael Feuerbacher[d,**], Janez Dolinšek[a,e,*]

[a] *Jožef Stefan Institute, Solid State Physics Department, Jamova 39, SI-1000 Ljubljana, Slovenia*

[b] *Division of Material Science Research, Korea Basic Science Institute, Daejeon 305-333, Republic of Korea*

[c] *University of Ljubljana, Faculty of Chemistry and Chemical Technology, Večna pot 113, SI-1000 Ljubljana, Slovenia*

[d] *Institut für Mikrostrukturforschung, Forschungszentrum Jülich, D-52425 Jülich, Germany*

[e] *University of Ljubljana, Faculty of Mathematics and Physics, Jadranska 19, SI-1000 Ljubljana, Slovenia*

* Corresponding author. *E-mail address*: jani.dolinsek@ijs.si (J. Dolinšek).

** Corresponding author. *E-mail address*: m.feuerbacher@fz-juelich.de (M. Feuerbacher).

Abstract

Rare-earths-based hexagonal high-entropy alloys (HEAs) composed of the elements from the heavy half of the lanthanide series (from Gd to Lu, with the exception of Yb) and yttrium are much closer to an ideal solid solution than HEAs composed of other elements from the entire periodic system. Using the method of high-frequency levitation melting, three candidates for a physical realization of an ideal HEA were synthesized, an Y-Gd-Tb-Dy-Ho, a Gd-Tb-Dy-Ho-Lu and a Tb-Dy-Ho-Er-Tm, and a study of their structure and composition was performed to see how close to ideal HEA samples can be prepared. We found that all three HEAs exhibit a nanostructure of a hexagonal close-packed (hcp) matrix and rod-like cubic close-packed (ccp) precipitates of the lengths 200 – 600 nm and widths 50 – 100 nm. EDS analysis has revealed a general trend that the precipitates are slightly enriched in the elements with larger atomic radii relative to the matrix. The origin of the nanostructure that represents a local hcp ↔ ccp polymorphism at zero external pressure appear to be lattice distortions (equivalent to a chemical pressure), occurring due to the minute differences of the elements' atomic radii. The volume per atom is slightly larger in the ccp precipitates that are enriched in larger atoms, so that the lattice distortions can be better accommodated and minimized, which reduces the lattice strain energy that contributes to the mixing enthalpy $\Delta H_{mix} \neq 0$. The employed synthesis route, which is standard for the preparation of alloys of high structural quality, did not lead to a physical realization of an ideal HEA in the most promising theoretical candidates.

Keywords: High-entropy alloys, rare-earths-based alloys, nanostructure, polymorphism.

1. Introduction

An ideal solution or ideal mixture is by definition a mixture of different kinds of molecules, where the molecular forces are the same between every pair of molecular kinds (like and unlike), so that there is no enthalpy of mixing, $\Delta H_{mix} = 0$. The Gibbs free energy of mixing contains the entropy term only, $\Delta G_{mix} = -T\Delta S_{mix}$, where the mixing entropy of an N-component mixture is $\Delta S_{mix} = -R\sum_{i=1}^{N} c_i ln c_i$ and c_i is the molar concentration of the component i. Mixing of the components in an ideal solution is completely random and a disordered solution is thermodynamically stable down to the lowest temperature. High-entropy alloys (HEAs) are multicomponent ($N \geq 5$) near-equiatomic alloys, which form mostly solid solutions including random solid solutions and partially ordered ones. An ideal HEA would be a single-phase, crystalline solid solution with no enthalpy of mixing and random distribution of the elements on an undistorted lattice. The absence of lattice distortions would require mixing the elements with equal atomic radii and the same bonding energy between the neighbors, so that there would be no strain energy that also contributes to ΔH_{mix}. In non-ideal ("regular") solutions, the interactions between unlike molecules are different from those between like molecules, and different atomic sizes distort the lattice, where both effects contribute to a non-zero mixing enthalpy, $\Delta H_{mix} \neq 0$. Positive ΔH_{mix} causes incomplete miscibility and leads to phase segregation, whereas negative ΔH_{mix} leads to the formation of intermetallic compounds. Mixing of the elements under the condition $\Delta H_{mix} \neq 0$ is non-random, so that preferential chemical environments are formed in the crystal lattice on the scale of nearest neighbors [1-3], at least in a HEA material that has been thermally annealed just below the melting temperature.

While the HEAs composed of 3*d*, 4*d* and 5*d* transition elements, sometimes alloyed with additional elements like Al, B and Si, all belong to the class of regular solutions that generally possess inhomogeneous micro- and nanostructure, rare-earths (RE)-based HEAs composed of the elements from the heavy half of the lanthanide series (from Gd to Lu, with the exception of Yb[§]) and yttrium appear to be close to an ideal HEA [4-8]. Pure elements all crystallize in the hexagonal close-packed (hcp) structure, the binary mixing enthalpies ΔH_{mix}^{ij} of any pair of the elements i and j are zero [9], all elements possess a 3+ valence in the crystalline state and their electronegativities are similar. Being neighbors in the periodic system, the atomic radii r_i of the lanthanides are very similar, showing slight contraction towards the heavier RE elements, whereas the atomic radius of Y is only slightly larger [9]. Consequently, the atomic-size-difference (geometric) parameter $\delta = \sqrt{\sum_{i=1}^{N} c_i(1 - r_i/\bar{r})^2}$ (where $\bar{r} = \sum_i c_i r_i$ is the composition-averaged atomic radius) of an equiatomic mixture of the RE elements is below 1 % for all the so far reported HEAs composed of Gd, Tb, Dy, Ho, Er, Tm, Lu and Y [4-8], reaching the smallest value of $\delta = 0.48$ % for the Tb-Dy-Ho-Er-Tm HEA [8]. This is much smaller than in the transition-metals-based regular HEAs, where the values of δ up to 6.5 % are found generally [10-12] and up to 3.8 % for the single-phase HEAs [13]. As compared to the regular HEAs, the lattice distortion effect in the hexagonal RE-based HEAs is minute, though still present. The composition-averaged theoretical hcp lattice parameters $\bar{a}$ and $\bar{c}$ of the reported RE-based HEAs [4-8] match almost perfectly the experimental a and c values, supporting random mixing of the elements on an almost undistorted lattice. All these facts are in favor of the hypothesis that the RE-based hexagonal HEAs composed of the elements from the heavy half of the lanthanide series (except Yb) and Y are close to a physical realization of an ideal HEA.

A literature report [4] on the Y-Gd-Tb-Dy-Lu and Gd-Tb-Dy-Tm-Lu polygrain samples (with the grains' size of 100 μm or less) from the potential class of "ideal" HEAs, prepared by arc-melting in an Ar atmosphere with repeated remelting and flipping of the ingots upside-down has revealed that the materials contained a high concentration of needle-shaped inclusions within the majority hcp matrix. The needles of about 10 μm length were visible already by an optical microscope and were observed inside the whole of the grains. Upon annealing for 1h@1273 K and 1day@1173 K, their concentration was somewhat reduced, but did not disappear. The inclusions could not be clearly observed in the SEM backscattered-electron (BSE) images and EDS elemental maps due to a too low contrast, indicating very similar chemical composition of the inclusions and the matrix. EDS has shown that the boundaries between the grains were strongly depleted in Y and Lu, whereas the grains were consequently enriched in these elements. The investigated Y-Gd-Tb-Dy-Lu and Gd-Tb-Dy-Tm-Lu polygrain HEA materials were thus quite far from an ideal HEA.

In another study [5], Y-Gd-Tb-Dy-Ho hcp HEA samples were prepared in a high-frequency levitation furnace under 1 bar Ar atmosphere. The ingots were remelted four times to achieve proper homogenization of the material and the cooling rate to room temperature was sufficiently slow to allow for the formation of a homogeneous single phase. The SEM BSE images have revealed a single-phase material, perfectly homogeneous on both 100 μm and 1 μm scale, with the absence of any compositional variation, precipitation of secondary phases and dendrite formation. High-angle annular dark field (HAADF) atomic-resolution *Z*-contrast images in a scanning transmission electron microscope (STEM) indicated that the material was homogeneous also on the 1 nm scale, suggesting an ideal solid solution with completely random mixing of the elements on any spatial scale. However, later additional studies of the same material by HAADF STEM imaging have revealed the presence of rod-like precipitates of several 100-nm length (Fig. 1a),

which could have been missed in the previous investigations. It is the purpose of this work to characterize these rod-like precipitates within the hcp matrix to find out (1) their structure (i.e., whether the HEA material is single-phase or two-phase), (2) their chemical composition and (3) to see whether they are present only in the investigated Y-Gd-Tb-Dy-Ho hcp HEA, or they form also in other RE-based alloys from the potential class of "ideal" HEAs. With other words, we address the question on how close to ideal HEA samples can be synthesized by the employed levitation melting synthesis route.

2. Materials and Methods

Our structural and compositional study on the sub-micrometer scale has included three candidates for an ideal HEA, an Y-Gd-Tb-Dy-Ho (in the following abbreviated as HEA-Y) [6], a Gd-Tb-Dy-Ho-Lu (HEA-Lu) [7] and a Tb-Dy-Ho-Er-Tm (HEA-ErTm) [8], for which complex magnetic phase diagrams were reported recently. The properties of pure elements constituting the investigated HEAs are given in Table 1. The atomic radii of the heavy lanthanides from Gd to Lu are in the range 1.78 – 1.73 Å [9], whereas Y is a bit larger atom with the radius of 1.82 Å. XRD patterns, presented in refs. [6-8] reveal a hcp structure (space group $P6_3/mmc$). The a and c lattice parameters are in good agreement with the composition-averaged theoretical values $\bar{a}$ and $\bar{c}$ (Table 1), supporting random mixing of the elements. The samples were explored using a HAADF STEM imaging technique on lamellae cut with a gallium beam in a Focused Ion Beam (FIB) instrument. HAADF STEM micrographs were obtained by a Jeol JEM-ARM 200F microscope. Samples for TEM were prepared by the Quanta 3D FEG FEI instrument. After the first experiments, the samples were additionally thinned in the FIB, to reach atomic resolution. The final sample

thickness in the analyzed areas was about 10 nm. For the FFT analysis, the DigitalMicrograph, Gatan Microscopy Suite, Version 3 software was used.

3. Results

The HAADF images of the three investigated HEAs, taken at room temperature, are shown in Fig. 1. For all three samples it is observed that rod-like precipitates are present within the alloy matrix. The lengths of the rods are distributed in the range 200 – 600 nm, whereas their widths are in the range 50 – 100 nm.

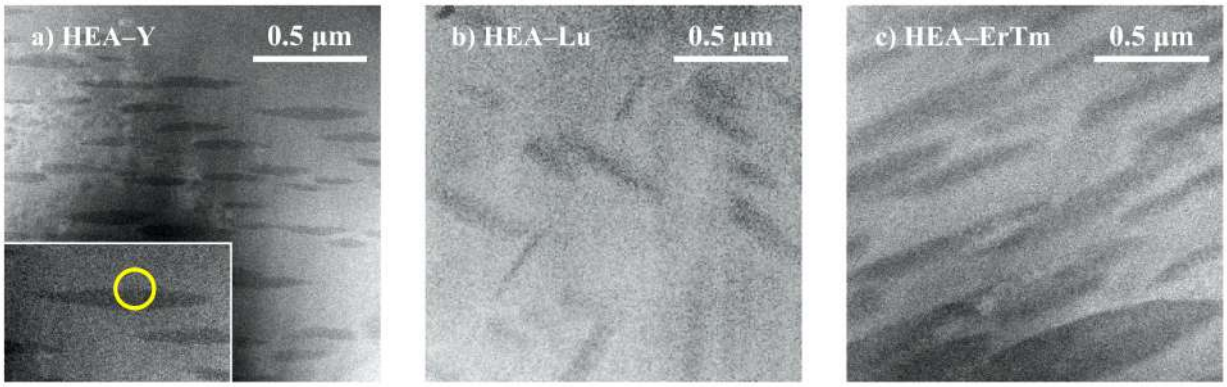

Fig. 1. HAADF images of **(a)** Y-Gd-Tb-Dy-Ho (HEA-Y), **(b)** Gd-Tb-Dy-Ho-Lu (HEA-Lu) and **(c)** Tb-Dy-Ho-Er-Tm (HEA-ErTm). Yellow circle in the inset of panel (a) designates the analysis area for the FFT to calculate the electron diffraction patterns.

The precipitates are a bit darker than the matrix and differ slightly in composition, as revealed by the STEM EDS analysis presented in Table 2. In the HEA-Y, the precipitates are slightly enriched in the largest atom yttrium (by about 3 %) with respect to the matrix, which is compensated by a decrease in the concentration of the smaller atoms Tb, Dy and Ho. In the HEA-Lu, the precipitates

are also enriched in the larger atoms with respect to the matrix, which is here realized by a decreased concentration of the smallest atom Lu (by about 1.1 %) in the precipitates. The HEA-ErTm is composed of the five elements with almost the same atomic radii (between 1.76 and 1.74 Å), so that a distinction between "smaller" and "larger" atoms is less obvious. From the EDS analysis it can still be concluded that the precipitates are slightly enriched in the largest atom Tb (by about 1 %), compensated by an equal decrease in the concentration of the smallest atom Er (an increase of the Dy concentration in the precipitates is almost perfectly compensated by a decrease of the Ho concentration, where Dy and Ho possess equal atomic radii). The EDS analysis thus reveals a general trend that the precipitates are slightly enriched in the larger atoms relative to the matrix.

The crystal phases of the matrix and the rod-like precipitates were identified for the HEA-Y, in which the enrichment in larger atoms of the precipitates with respect to the matrix is most pronounced. The analysis area in the HAADF STEM image that contains both the precipitate and the matrix is marked by a yellow circle in the inset of Fig. 1a. Fast Fourier transforms (FFT) of the selected areas (one for the matrix and one for the precipitate) were calculated to produce electron diffraction patterns. Since the XRD analysis [6] has shown that the matrix possesses a hcp structure with the unit cell parameters $a = 3.61$ Å and $c = 5.70$ Å, we have used the structure of hexagonal Dy ($a = 3.59$ Å, $c = 5.65$ Å, PDF card 00-015-0430) with the cell parameters close enough to the ones of the HEA-Y for the interpretation of the diffraction pattern. Fig. 2 shows that the calculated diffraction pattern of the matrix can be well explained by a simulated diffraction pattern of the Dy hcp phase along the [100] zone axis. The same procedure was then applied to the precipitate. Here, however, it was not possible to index the calculated diffraction pattern of the precipitate (Fig. 2) by the hcp structure. Successful indexing was only possible by a simulated diffraction pattern of a

cubic close-packed[†] (ccp) Dy, having the unit cell parameter of 5.18 Å (space group F$m\bar{3}m$, PDF card 04-003-4708). The simulated diffraction pattern of the ccp Dy along the [011] zone axis is also shown in Fig. 2.

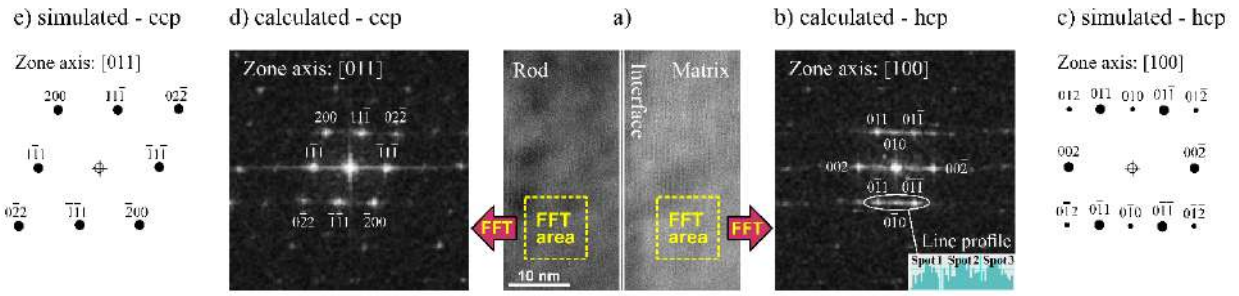

Fig. 2. Identification of crystal phases of the matrix and the rod-like precipitate for the HEA-Y. Middle panel **(a)** shows the HAADF STEM image of the interface region. Yellow squares mark selected areas used to calculate the electron diffraction patterns by a FFT procedure. Panel **(b)** shows the indexed calculated diffraction pattern of the matrix phase, whereas in panel **(c)**, the simulated diffraction pattern of the Dy hcp phase along the [100] zone axis is shown. The inset at the bottom of panel (b) shows the evidence of a clearly present $0\bar{1}0$ reflection (spot 2), which is important to identify the hcp phase. Panel **(d)** shows the indexed calculated diffraction pattern of the rod-like precipitate, whereas in panel **(e)**, the simulated diffraction pattern of the Dy ccp phase along the [011] zone axis is shown.

To determine the structural relationship between the matrix and the precipitate, the HAADF image of the interface region was analyzed. The FFT of the image, representing a calculated diffraction pattern, could be indexed by an overlay of diffraction patterns of the cubic (zone axis [011]) and hexagonal (zone axis [100]) phases (Fig. 3, left panel). An indication, which spots belong to the cubic and which to the hexagonal phase is also given. Overlaid simulated diffraction patterns of

the Dy hcp and ccp phases along the [100] and [011] zone axes, respectively, are shown in the right panel of Fig. 3. The blue circle in the simulated image embeds two spots that nearly coincide and represent the cubic $00\bar{2}$ and the hexagonal $\bar{1}1\bar{1}$ reflections. These two reflections (and the equivalent 002 and $1\bar{1}1$) are attributed to the combined atomic plane where the ccp and the hcp structures merge.

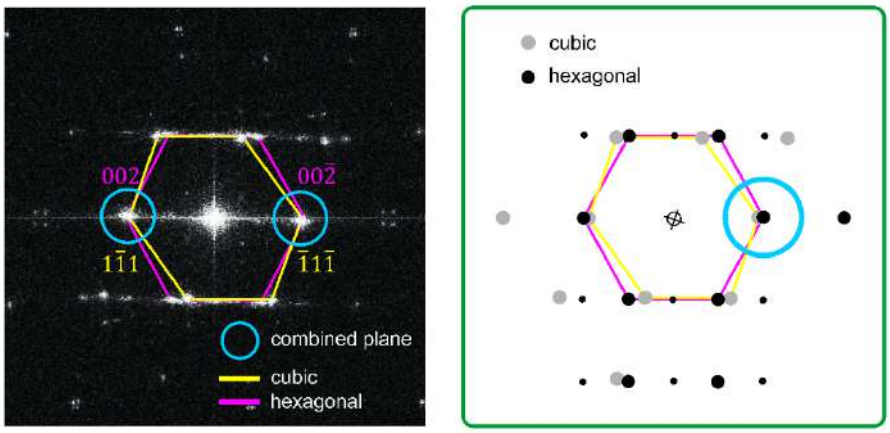

Fig. 3. Calculated diffraction pattern of the interface region (left panel) with indication, which spots belong to the cubic and which to the hexagonal phase and overlaid simulated diffraction patterns (right panel) of the Dy hcp and ccp phases along the [100] and [011] zone axes, respectively. The blue circle in the right image embeds two spots that nearly coincide and represent the cubic $00\bar{2}$ and the hexagonal $\bar{1}1\bar{1}$ reflections.

A HAADF image of the interface region in the direct space is presented in the left panel of Fig. 4, showing how the two phases are spatially related. The two insets in the middle show atomic resolution projection of the ccp precipitate along the [011] zone axis and the hcp matrix along the [100] zone axis. The inset at the bottom shows the atomic structure projection of the interface. In the right panel of Fig. 4, a schematic representation of the atomic arrangement at the interface is shown. The crystal planes of the type (001) of the hexagonal matrix and (111) of the cubic

precipitate are parallel to each other and one such plane represents the interface. This situation is common for such types of structures as these planes are all close-packed ones, present in both the ccp and the hcp structures. The discriminating difference between the two structures is the stacking order ABABAB for the hexagonal and ABCABC for the cubic. It is thus natural that one such plane forms the interface, where the stacking sequence on one side of the interface plane goes ABCABC and on the other ABABAB.

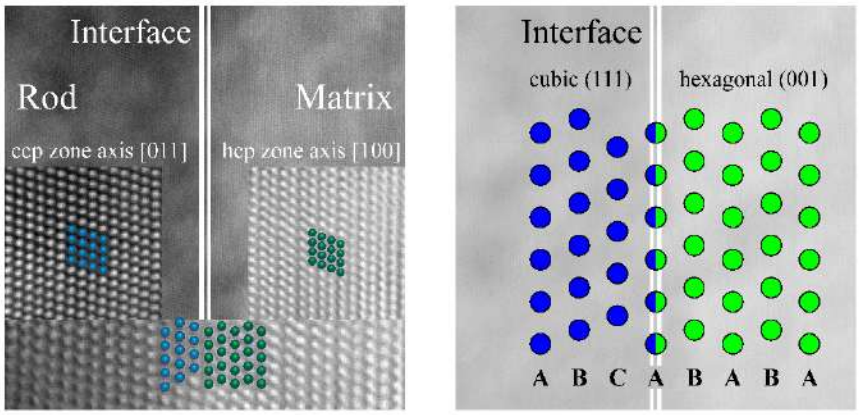

Fig. 4. HAADF image of the interface region in the direct space (left panel), showing how the two phases are spatially related. The two insets in the middle show atomic-resolution projection of the ccp precipitate along the [011] zone axis and the hcp matrix along the [100] zone axis. The inset at the bottom shows the atomic structure projection of the interface. Right panel shows a schematic representation of the atomic arrangement at the interface. The crystal planes of the type (001) of the hexagonal matrix and (111) of the cubic precipitate are parallel to each other and one such plane represents the interface.

In principle, the interplanar spacing d of the two structures could be equal (i.e. the d_{111} (cubic) and d_{002} (hexagonal) would have the same value). It is, however, normally not the case. Based on the known data of the hexagonal and cubic Dy given above (as an approximation of the HEA-Y),

the expected simulated mismatch would be $\varepsilon = -5.6$ %, where the mismatch is defined as $\varepsilon = (d_{matrix} - d_{prec})/d_{matrix}$ and the values are $d_{matrix} = 2.83$ Å for the hexagonal matrix and $d_{prec} = 2.99$ Å for the cubic precipitate. Measurement of the corresponding d values of the reflections, identified in the calculated diffraction images of the HEA-Y yielded the values of 2.96 and 3.08 Å for the matrix and the precipitate, respectively, from which the calculated mismatch is $\varepsilon = -4.0$ %. The mismatch of the interplanar spacing of the hexagonal matrix and the cubic precipitate produces mechanical strain at the interface between the two phases.

The HAADF STEM images and the analysis presented in Figs. 1–4 clearly reveal the presence of the ccp precipitates on the 100-nm scale within the hcp matrix. However, the XRD pattern of the same HEA-Y material published in the preceding publication [6] has shown only the reflections of the hcp structure, with no unidentified reflections left that could be indexed to the ccp phase. To clarify this discrepancy, the measurement of the XRD pattern has been repeated after a thorough metallographic preparation of the sample's surface (polishing first with polishing papers and then with a diamond paste of 250 nm grains size). The result is shown in Fig. 5. In addition to the hcp reflections, a careful inspection reveals a weak reflection at 29.7° (inset in Fig. 5), which is attributed to the 111 reflection of the ccp phase (space group F$m\bar{3}m$) with the unit cell parameter $a = 5.21$ Å. The positions of other ccp reflections (all of very weak intensity) are indicated in Fig. 5 by dashed vertical lines, where it can be noticed that they are in most cases hidden behind the high-intensity hcp reflections. The absence of the 200 ccp reflection expected at 34.4° is very likely a consequence of preferential orientation of the precipitates along the [111] crystallographic direction. The XRD pattern of Fig. 5 thus confirms the presence of the ccp precipitates within the hcp matrix, but the total volume of the precipitates is small. Here it is important to recall that the X rays penetrate into the bulky metallic specimen only to the depth of

a few micrometers, so that the very small total volume of the ccp precipitates can be claimed for the irradiated surface layer, but may be different in other parts of the sample.

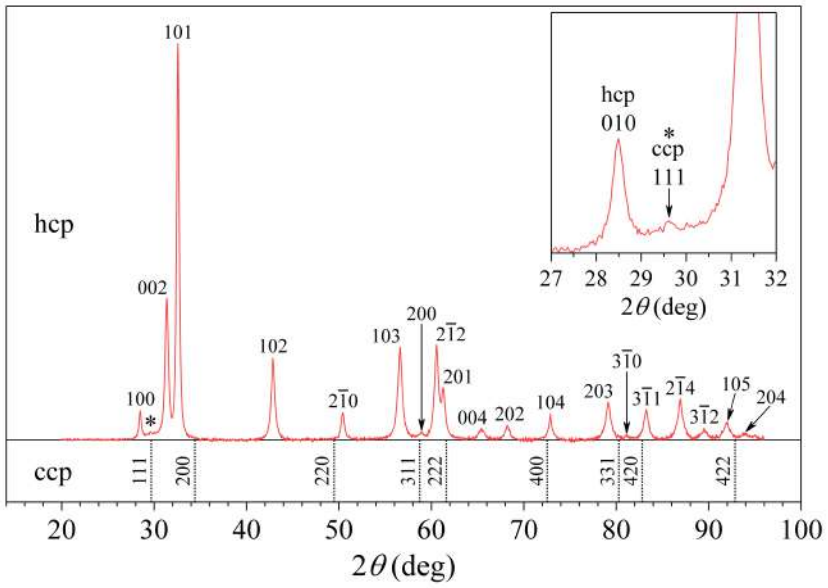

Fig. 5. XRD pattern of the HEA-Y sample. Miller indices of the hcp reflections are written on the peaks. The weak 111 reflection of the ccp phase at 29.7° (marked by an asterisk) is clearly visible in the inset. The expected positions of the ccp reflections (space group $Fm\bar{3}m$, $a =$ 5.21 Å) are marked by the vertical dashed lines.

4. Discussion

The observed nanostructure of the rod-like ccp precipitates within the majority hcp matrix reveals local polymorphism. The investigated HEA-Y material is not single-phase, but a hcp – ccp mixture, metastable perhaps. Since the HAADF images of the HEA-Lu and HEA-ErTm presented in Fig. 1 also show the nanostructure of rod-like precipitates within the hcp matrix, the two-phase mixed state exists in these HEAs as well. As already mentioned, the ccp and the hcp structures

differ only in the stacking sequence of the same hexagonal close-packed atomic layers, so that one type of a structure can readily be obtained locally from the other by introducing stacking faults. Such transformation requires only small atomic displacements associated with the formation of stacking faults. The detailed mechanism of the hcp ↔ ccp nanoscale polymorphic transition could be more complex since stacking faults (planar defects), dislocations (linear defects) and twinning events may all be involved [14-17].

In crystals, the polymorphic transition is usually triggered by pressure or temperature. The magnetic state of the material can affect the transition as well. The decisive role of the external pressure on the ccp ↔ hcp polymorphic transition in regular HEAs composed of the 3*d* magnetic transition elements was already demonstrated for the CoCrFeMnNi, which is ccp at ambient pressure, but transforms into a hcp structure under pressure [18,19]. The phase transition is sluggish, starting at ∼22 GPa and almost completes at ∼41 GPa. By releasing the pressure, the high-pressure hcp phase is retained to zero pressure, demonstrating irreversibility of the transition and suggesting very similar free energies of the ccp and hcp phases and/or a large potential barrier between them. The polymorphic transition in the CoCrFeMnNi HEA can easily be realized due to the low stacking fault energy of ∼20 mJm^{-2} in this material [20], which facilitates sliding of the close-packed atomic planes needed for a displacive phase transition.

In our investigated RE-based HEAs, the hcp ↔ ccp polymorphic transition occurs locally on the 100-nm scale at zero external pressure. Lattice distortions due to unequal atomic radii of the employed RE elements seem to play a decisive role in the selection of the polymorph type. Such distortions can be associated with local internal (chemical) pressure. A hint comes from thin films of Gd, Tb, Dy, Ho, Er and Tm, which all crystallize in the ccp structure at the thickness of 14 nm, thicker films (20 nm) are a mixture of the ccp and hcp phases, whereas thick films contain

the hcp phase only, like the bulk metals [21]. The polymorphism (more precisely the allotropy) at zero external pressure in thin films of pure heavy-RE elements appears to be a nanoscale effect and can be associated with lattice distortions, although all the atoms in a given film possess the same radius. The surface atomic monolayer exhibits broken symmetry because of a reduced nearest-neighbor coordination, which then extends to several monolayers beneath due to a structural relaxation normal to the surface. The lattice distortions introduce mechanical strains and trigger the allotropic transition.

In bulk crystals, the dependence of the crystal structure on pressure originates from the fact that the pressure alters lattice constants and hence the volume of the unit cell. The volume changes transform physical parameters, which affect the electrostatic potential energy of a solid, so that different crystal structures may have the lowest energy at different pressure ranges. The externally applied pressure (also called physical pressure) always results in a reduction of the unit cell volume. In substitutionally disordered crystals, random distribution of the atoms with different atomic radii locally expands or contracts the lattice. The associated local volume changes in the lattice are interpreted as a chemical pressure, which can be either positive or negative. The chemical pressure introduces local strains in the lattice, which increase the enthalpy of mixing ΔH_{mix} of a substitutionally disordered crystal. In HEAs, the substitutional (chemical) disorder is immense, so that the associated chemical pressure in the lattice can be substantial.

In the HEA-Y, the precipitates are slightly enriched in the biggest element Y by about 3 % relative to the matrix. This increases the lattice distortion energy and hence ΔH_{mix} of the localized nanoscale volume with the enriched yttrium concentration. It is energetically favorable for this localized volume to transform from the hcp structure with the volume per atom $V_{atom}^{hcp} = 32.2$ Å^3 (following from the unit cell parameters $a = 3.61$ Å and $c = 5.70$ Å that yield the unit cell volume

$V_{cell}^{hcp} = 64.33$ Å^3, with two atoms per cell) to a ccp structure with a larger volume per atom $V_{atom}^{ccp} =$ 35.4 Å^3 (following from $a = 5.21$ Å that yields $V_{cell}^{ccp} = 141.4$ Å^3, with four atoms per cell), where the relative volume-per-atom enlargement amounts to $\Delta V/V = \left(V_{atom}^{ccp} - V_{atom}^{hcp}\right)/V_{atom}^{hcp} = 3.4$ %. In a structure with an enlarged atomic volume, the lattice distortions can be better accommodated and minimized, which reduces the lattice strain energy contribution to the mixing enthalpy ΔH_{mix}. The hcp ↔ ccp polymorphic transition within the local volume enriched in the largest atom yttrium reduces the lattice strain energy within the entire ccp precipitate. The energetic "bill" is partially paid at the interface between the two phases, where the mismatch ε of the interplanar spacing of the hexagonal matrix and the cubic precipitate produces mechanical strain and increases the lattice strain energy of the interface. However, the decrease of the strain energy within the entire volume of the ccp precipitate (of typical lengths 200 – 600 nm and widths 50 – 100 nm) is larger than the increase of the strain energy within the interface, which takes place only within the first few atomic monolayers beneath the interface atomic plane due to a structural relaxation normal to that plane. The situation is somewhat analogous to the formation of magnetic domains in ferromagnets, where the domain structure minimizes the long-range magnetic dipole interaction between the magnetic moments within the entire volume of the domains, at the expense of a smaller increase of the electrostatic exchange energy within the domain walls. In a certain sense, chemical pressure (denoting random local changes of the unit cell volume) in the substitutionally disordered HEA lattice triggers the local polymorphic transition at zero external pressure. Since the HEA-Lu and HEA-ErTm also comply with the general trend that the precipitates are slightly enriched in larger atoms with respect to the matrix, the origin of the rod-like precipitates within the hcp matrix (Fig. 1) can be considered to be the same as in the HEA-Y.

The question whether the experimentally observed very small differences in composition can indeed produce sufficient strain energy to trigger local polymorphism and a two-phase structure can be assessed qualitatively by considering compressibility of the constituent RE elements in the metallic state under external pressure. The relative volume change under pressure Δp can be estimated from the equation $\Delta V/V = \Delta p/K$, where K denotes bulk modulus of the material. The bulk moduli of the elements Y, Gd, Tb, Dy and Ho are all in the range $K = 38 – 41$ GPa. Taking the value $K = 40$ GPa for an estimate, we find that the relative volume change by 3.4 % would correspond to a pressure $\Delta p = 1.36$ MPa. This value falls into the range of pressures (0.8 – 2.5 GPa) within which the pure Gd and Tb metals undergo a pressure-induced polymorphic transition from hcp to a Sm-type rhombohedral phase at temperatures between RT and the melting temperature [22]. The hypothesis that chemical pressure is at the origin of local polymorphism in the investigated HEAs is thus plausible.

Theoretically, the relative stability of the ccp and the hcp phases of hard spheres is a long-standing problem in statistical physics. Finding the difference in the free energy between the two structures of identical packing densities (identical close-packed volumes) and very similar equations of state [23] has been the objective of much theoretical [24,25] and computational [26-28] effort, but without a conclusive resolution. It was proposed that the ccp ↔ hcp transition could be entropy dominated [29]. Since HEAs possess an extremely high mixing entropy, the RE-based HEAs can provide convenient model systems for exploring the fundamental question of the relative stability of the ccp and hcp packing.

5. Conclusions

As to the basic question on how close to ideal HEA materials from the potential class of "ideal" RE-based alloys can be grown in the laboratories, our three investigated HEAs all fail to satisfy the criterion of a single-phase material, by exhibiting a nanostructure of the hcp matrix and the ccp precipitates. The origin of this nanoscale local polymorphism at zero external pressure appear to be tiny compositional inhomogeneities on the 100-nm scale, where in some regions, the concentrations of the elements with slightly bigger or smaller atomic radii are enriched by up to a few at. %. The differences of the RE elements' atomic radii are indeed minute, but still large enough to produce lattice distortions (equivalent to the chemical pressure) that create sufficient strain energy to induce local polymorphism and a two-phase nanostructure. Consequently, though the binary mixing enthalpies of any pair of the employed RE elements are zero, $\Delta H_{mix}^{ij} = 0$, the total mixing enthalpy is nonzero, $\Delta H_{mix} \neq 0$, due to the lattice strain energy contribution. The investigated RE-based HEAs thus fail to satisfy the $\Delta H_{mix} = 0$ criterion of an ideal solution and the physical realization of an ideal HEA is not met even in the best theoretical candidates.

It is important to emphasize that the above conclusion is valid for the samples produced by the employed synthesis route, using the high-frequency levitation melting technique, by remelting the samples four times and flipping them upside-down, followed by slow cooling to room temperature. Such a synthesis route is standard for the preparation of alloys of high structural quality. The two-phase mixed state is, however, not expected to be the ground state of the investigated materials. Longer melting time, larger number of the remelting cycles and slower cooling to room temperature may result in a closer-to-ideal random distribution of the elements and a single-phase structure. Long thermal annealing may also tend to dissolve the ccp precipitates, but due to the relatively large volumes of the precipitates and the fact that thermal diffusion of the heavy RE elements is sluggish, the material may be effectively trapped into the metastable two-

phase mixed state for macroscopically long times. Other synthesis methods like Czochralski and Bridgman growth may also yield a closer-to-ideal, single-phase hcp HEA material.

Acknowledgements

The Slovenian authors acknowledge the financial support from the Slovenian Research Agency (research core funding No. P1-0125). MF acknowledges financial support from the German Research foundation (DFG) under grant No. FE 571/4 within the priority program SPP2006 "Compositionally Complex Alloys – High Entropy Alloys (CCA-HEA)". We thank Dr. Ji Hyun Lee from KBSI Daejeon for the FIB lamella preparation.

Table 1. Structural properties of pure RE elements in the metallic state and the Y-Gd-Tb-Dy-Ho (HEA-Y), Gd-Tb-Dy-Ho-Lu (HEA-Lu) and Tb-Dy-Ho-Er-Tm (HEA-ErTm) alloys [30]. Atomic radii were taken from [9]. Theoretical lattice parameters of the HEAs were calculated by the Vegard's rule of mixtures.

	Y	Gd	Tb	Dy	Ho	Er	Tm	Lu	HEA-Y		HEA-Lu		HEA-ErTm	
									exp.	theory	exp.	theory	exp.	theory
Structure (300 K)	hcp	hcp	hcp	hcp	hcp	hcp	hcp	hcp	hcp		hcp		hcp	
a (Å)	3.650	3.634	3.606	3.592	3.578	3.559	3.538	3.505	3.61	3.613	3.59	3.585	3.58	3.575
c (Å)	5.734	5.781	5.697	5.650	5.618	5.585	5.554	5.549	5.70	5.698	5.66	5.662	5.63	5.622
Atomic radius (Å)	1.82	1.78	1.76	1.75	1.75	1.74	1.76	1.73						

Table 2. STEM EDS-determined composition of the matrix and the rod-like precipitates (in at.%). The rod – matrix difference in composition is also given. Each composition is an average of typically 10 measurements at closely spaced spots (the error is estimated to be about ± 0.3).

	HEA-Y				
	Y	Gd	Tb	Dy	Ho
rod	25.7	17.2	18.6	18.6	19.9
matrix	22.8	17.1	19.2	19.9	21.0
rod – matrix	**+2.9**	**+0.1**	**–0.6**	**–1.3**	**–1.1**
	HEA-Lu				
	Gd	Tb	Dy	Ho	Lu
rod	17.9	20.1	21.7	22.8	17.5
matrix	17.9	19.7	21.0	22.7	18.7
rod – matrix	**0.0**	**+0.4**	**+0.7**	**+0.1**	**-1.2**
	HEA-ErTm				
	Tb	Dy	Ho	Er	Tm
rod	20.0	21.8	20.8	20.4	17.0
matrix	18.9	21.1	21.5	21.4	17.1
rod – matrix	**+1.1**	**+0.7**	**–0.7**	**–1.0**	**–0.1**

Data availability

The raw data required to reproduce these findings cannot be shared at this time due to technical or time limitations. The processed data required to reproduce these findings cannot be shared at this time due to technical or time limitations.

References

§ Yb crystallizes at room temperature in a face-centered cubic structure and its binary mixing enthalpy with other RE elements from the heavy-half of the lanthanide series is nonzero (positive).

† A cubic close-packed (ccp) structure is equivalent to a face-centered cubic (fcc) structure.

[1] L.J. Santodonato, Y. Zhang, M. Feygenson, C.M. Parish, M.C. Gao, R.J.K. Weber, J.C. Neuefeind, Z. Tang, and P.K. Liaw, Nat. Commun. **6**, 5964 (2015).

[2] S. Vrtnik, P. Koželj, A. Meden, S. Maiti, W. Steurer, M. Feuerbacher, J. Dolinšek, J. Alloys Compd. **695**, 3530 (2017).

[3] P. Koželj, S. Vrtnik, A. Jelen, M. Krnel, D. Gačnik, G. Dražić, A. Meden, M. Wencka, D. Jezeršek, J. Leskovec, *et al*., Adv. Eng. Mater. 1801055 (2019), DOI: 10.1002/adem.201801055.

[4] A. Takeuchi, K. Amiya, T. Wada, K. Yubuta, W. Zhang, JOM **66**, 1984 (2014).

[5] M. Feuerbacher, M. Heidelmann, C. Thomas, Mat. Res. Lett. **3**, 1 (2014).

[6] J. Lužnik, P. Koželj, S. Vrtnik, A. Jelen, Z. Jagličić, A. Meden, M. Feuerbacher, J. Dolinšek, Phys. Rev. B **92**, 224201 (2015).

[7] S. Vrtnik, J. Lužnik, P. Koželj, A. Jelen, J. Luzar, M. Krnel, Z. Jagličić, A. Meden, M. Feuerbacher, and J. Dolinšek, Intermetallics **105**, 163 (2019).

[8] M. Krnel, S. Vrtnik, A. Jelen, P. Koželj, Z. Jagličić, A. Meden, M. Feuerbacher, J. Dolinšek, Intermetallics **106**, 106680 (2020).

[9] A. Takeuchi, A. Inoue, Mat. Trans. **46**, 2817 (2005).

[10] Z. Wang, S. Guo, C.T. Liu, JOM **66**, 1966 (2014).

[11] Y. Zhang, Y.J. Zhou, J.P. Lin, G.L. Chen, P.K. Liaw, Adv. Eng. Mater. **10**, 534 (2008).

[12] S. Guo, C.T. Liu, Chin. J. Nat. **35**, 85 (2013).

[13] D.B. Miracle, J.D. Miller, O.N. Senkov, C. Woodward, M.D. Uchic, J. Tiley, Entropy **16**, 494 (2014).

[14] D. Ma, B. Grabowski, F. Körmann, J. Neugebauer, D. Raabe, Acta Mater. **100**, 90 (2015).

[15] F. Tian, L.K. Varga, J. Shen, L. Vitos, Comput. Mater. Sci. **111**, 350 (2016).

[16] M. Jo, J.M. Koo, B.-J. Lee, B. Johansson, L. Vitos, S.K. Kwon, Proc. Natl. Acad. Sci. USA **111**, 6560 (2014).

[17] W. Li, S. Lu, Q.M. Hu, B. Johansson, S.K. Kwon, M. Grehk, J.Y. Johnsson, L. Vitos, Philos. Mag. **96**, 524 (2016).

[18] C.L. Tracy, S. Park, D.R. Rittman, S.J. Zinkle, H. Bei, M. Lang, R.C. Ewing, W.L. Mao, Nat. Commun. **8**, 15634 (2017); doi: 10.1038/ncomms15634.

[19] F. Zhang, Y. Wu, H. Lou, Z. Zeng, V.B. Prakapenka, E. Greenberg, Y. Ren, J. Yan, J.S. Okasinski, X. Liu, Y. Liu, Q. Zeng, Z. Lu, Nat. Commun. **8**, 15687 (2017); doi: 10.1038/ncomms15687.

[20] A.J. Zaddach, C. Niu, C.C. Koch, D.L. Irving, JOM **65**, 1780 (2013).

[21] A.E. Curzon, H.G. Chlebek, J. Phys. F: Metal Phys. **3**, 1 (1973).

[22] G.K. Samudrala, G.M. Tsoi, S.T. Weir, Y.K. Vohra, High Pressure Research **34**, 385 (2014).

[23] B.J. Alder, W.G. Hoover, D.A. Young, J. Chem. Phys. **49**, 3688 (1968).

[24] F.H. Stillinger, Z.W. Salsburg, J. Chem. Phys. **46**, 3962 (1967).

[25] W.G. Rudd, Z.W. Salsburg, A.P. Yu, F.H. Stillinger, J. Chem. Phys. **49**, 4857 (1968).

[26] B.J. Alder, B.P. Carter, D.A. Young, Phys. Rev. **183**, 831 (1969).

[27] B.J. Alder, D.A. Young, M.R. Mansigh, Z.W. Salsburg, Comput. Phys. **7**, 361 (1971).

[28] D. Frenkel, A.J.C. Ladd, J. Chem. Phys. **81**, 3188 (1984).

[29] L.V. Woodcock, Nature **385**, 141 (1997); https://doi.org/10.1038/385141a0.

[30] J. Jensen, A.R. Mackintosh, *Rare Earth Magnetism* (Clarendon Press, Oxford, 1991), p. 17.